

# **Aerogel Growth, Optical Birefringence Characterization, and Use in Ultra Low Temperature Superfluid $^3\text{He}$ Experiments**

Senior Honors Thesis

Kent Shirer

Advisor: Prof. William Halperin

*Department of Physics and Astronomy*

*Northwestern University, Evanston, Illinois 60208*

## **Abstract**

Superfluid  $^3\text{He}$  has important implications in studying condensed matter physics, specifically in its phases at very low temperatures. The understanding of these phases not only expands our knowledge of  $^3\text{He}$  itself, but is also a paradigm for recently discovered unconventional superconductors such as strontium ruthenate ( $\text{SrRuO}_3$ ) and uranium platinum three ( $\text{UPt}_3$ ). Superfluid  $^3\text{He}$ 's relation to superconductors is not in its pure form, but in dirty superfluid  $^3\text{He}$ , where impurities from external sources are present. This is because real superconductors, unlike ideal ones, contain unavoidable impurities. In  $^3\text{He}$ , however, we can control the number of impurities and how they are distributed in space. These impurities are introduced by filling the extremely porous structure of silica aerogel with  $^3\text{He}$ . The aerogel pore size is on a scale that causes  $^3\text{He}$  particles to scatter, similar to the behavior brought about by impurities in other unconventional systems. The microstructure of the aerogel plays an integral role in the modification of the  $^3\text{He}$  system. Presented here are aerogel growth methods developed to control this microstructure, and the employment of optical birefringence as an aerogel characterization technique.

## **Introduction and Motivation**

### *Aerogel*

Silica aerogel is an extremely porous, low-density material, which is formed by synthesis of silica clusters that form a network of strands which have a diameter of approximately 3-5 nm and average separation of  $\xi \approx 30-100$  nm, called the correlation length [1]. The porosity of these gels can range up to approximately 99.5% and have been used in a vast array of scientific and engineering disciplines including civil and environmental engineering, chemical engineering, materials science, astrophysics, high-energy physics, and condensed matter physics. The extremely low thermal conductivity of silica aerogel has made it useful as insulation in civil and environmental engineering, with potential commercial applications [2]. In chemical engineering, silica aerogel can be engineered to include metal or metal oxide particles in its structure, often for use in catalysis [3]. Aerogels are significant in materials science for their fractally correlated structure [4] as well as their use in ceramics manufacture [5]. In astrophysics and particle physics, aerogels have found applications in the collection of cosmic dust from the 81P/Wild 2 comet by NASA [6] and the detection of Cerenkov radiation [7]. In condensed matter physics, aerogels have been used to understand the effect of impurities on phase transitions in liquid crystals, and, as in the case of this work, act as an impurity in superfluid  $^3\text{He}$  systems.

### *Optical Birefringence*

Optical birefringence is a well known characterization method for many materials, such as liquid crystals [8, 9]. A transparent material is birefringent if it possesses an anisotropic dielectric constant, which leads to the presence of an optical axis in the

material. The illumination of a material that is optically birefringent with white light results in transmission of two components with orthogonal polarizations, parallel and perpendicular to the optical axis. Birefringence can be explained by exploring how electromagnetic waves propagate in homogeneous, anisotropic dielectrics.

In a homogeneous isotropic dielectric,  $\vec{E}$ , the electric field strength and  $\vec{P}$ , the polarization vector, can be assumed to be parallel. In a homogeneous anisotropic dielectric, however, this assumption cannot be made and therefore the electric displacement  $\vec{D}$  must be written

$$\vec{D} = \epsilon_0 \vec{E} + \vec{P} \quad (1)$$

The three orthogonal components of  $\vec{D}$  can be related to those of  $\vec{E}$  by the following equations,

$$D_u = \kappa_1 \epsilon_0 E_u \quad D_v = \kappa_2 \epsilon_0 E_v \quad D_w = \kappa_3 \epsilon_0 E_w \quad (2)$$

For principle directions  $O_u$ ,  $O_v$ , and  $O_w$ . Where  $\kappa_1$ ,  $\kappa_2$ , and  $\kappa_3$  are the principle dielectric constants,

$$\kappa_1 = 1 + \frac{\chi_1}{\epsilon_0} \quad \kappa_2 = 1 + \frac{\chi_2}{\epsilon_0} \quad \kappa_3 = 1 + \frac{\chi_3}{\epsilon_0} \quad (3)$$

These conditions apply to all anisotropic dielectrics as long as the displacement  $\vec{D}$  is linear with the electric field strength and the dielectrics exhibit no distinguishable asymmetry between right-handed and left-handed forms.

To understand how plane waves propagate in anisotropic dielectrics, we look for solutions of Maxwell's equations in which the electric and magnetic vectors are only functions of  $x$  and  $t$ . To do this, we first assume a dielectric with  $\rho_f$  and  $J_f$  both equal to zero. Maxwell's equations then become,

$$\int_S D_n dS = 0 \quad (4)$$

$$\oint_S E_s ds = -\mu_0 \int_S \frac{\partial H_n}{\partial t} dS \quad (5)$$

$$\int_S H_n dS = 0 \quad (6)$$

$$\oint_S H_s ds = \int_S \frac{\partial D_n}{\partial t} dS \quad (7)$$

We can choose an arbitrary coordinate system, so we will take a Cartesian one.

Remembering that we want a solution only dependent on x and t, we can consider an area

S parallel to the yz-plane. In this plane  $\vec{E}$  is constant (because  $\rho_f = 0$ ) and so we have,

$$\oint_S E_s ds = 0 \quad (8)$$

Therefore,

$$\int_S \frac{\partial H_x}{\partial t} dS = 0 \quad (9)$$

And because  $H_x$  has the same value at all points on S,

$$\frac{\partial H_x}{\partial t} = 0 \quad (10)$$

Similarly,

$$\frac{\partial D_x}{\partial t} = 0 \quad (11)$$

If we apply equation (5) to a rectangle TUVW with two sides of infinitesimal length dx and parallel to the x-axis and two sides of length h parallel to the y-axis, where x is the x-coordinate of TW and x+dx is the x-coordinate of UV, then  $\vec{E}(x)$  has a constant value along TW and a different constant value  $\vec{E}(x+dx)$  along UV. Therefore, the line integral of  $\vec{E}$  along TUVW reduces to

$$\oint_S E_s ds = h[E_y(x+dx) - E_y(x)] \quad (12)$$

Thus

$$\oint_S E_s ds = h \frac{\partial E_y}{\partial x} dx \quad (13)$$

The right side of equation (5) represents the flux of  $d\vec{H}/dt$  through TUVW and can similarly be written

$$\int_S \frac{\partial H_n}{\partial t} dS = h \frac{\partial H_z}{\partial t} dx \quad (14)$$

And so

$$\frac{\partial E_y}{\partial x} = -\mu_0 \frac{\partial H_z}{\partial t} \quad (15)$$

Equation (5) can also be applied to a rectangle T'U'V'W' with sides parallel to the z- and x-axes. In this case we obtain, similarly

$$\frac{\partial E_z}{\partial x} = \mu_0 \frac{\partial H_y}{\partial t} \quad (16)$$

Equation (7) also allows us to obtain equations using the same rectangles used for equation (5). This gives us

$$\frac{\partial H_y}{\partial x} = \frac{\partial D_z}{\partial t} \quad (17)$$

And

$$\frac{\partial H_z}{\partial x} = -\frac{\partial D_y}{\partial t} \quad (18)$$

Two more equations can be obtained by using (4) and (6) using a parallel piped with a closed surface S. Where x and dx are the coordinates of the two planes TUVW and T'U'V'W' respectively, which are perpendicular to the x-axis. The lengths of the sides

parallel to the y- and z-axes are h and k respectively. The flux of D through T'U'V'W' will then be

$$D_x(x+dx)hk \quad (19)$$

And through TUVW it will be

$$-D_x(x)hk \quad (20)$$

The total flux through the sides perpendicular to the x-axis will be

$$hk[D_x(x+dx) - D_x(x)] = hk \frac{\partial D_x}{\partial x} dx \quad (21)$$

Because D is only dependent on x, the fluxes of D through surfaces TT'U'U and VV'W'W have equal magnitudes but opposite signs and therefore cancel each other. This is also true for the fluxes through UVV'U' and TWW'T'. Therefore, we have the equation,

$$\frac{\partial D_x}{\partial x} = 0 \quad (22)$$

In the same way

$$\int_S H_n dS = 0 \quad (23)$$

Gives us

$$\frac{\partial H_x}{\partial x} = 0 \quad (24)$$

The results from Maxwell's equations provide us with a system of differential equations which we will now use to explain the propagation of a wave in a homogeneous, anisotropic dielectric.

$$(a) \quad \frac{\partial H_x}{\partial x} = 0 \quad (b) \quad \frac{\partial D_x}{\partial x} = 0$$

$$\begin{aligned}
\text{(c)} \quad \frac{\partial H_x}{\partial t} &= 0 & \text{(d)} \quad \frac{\partial D_x}{\partial t} &= 0 & (25) \\
\text{(e)} \quad \frac{\partial E_z}{\partial x} &= \mu_0 \frac{\partial H_y}{\partial t} & \text{(f)} \quad \frac{\partial H_z}{\partial x} &= -\frac{\partial D_y}{\partial t} \\
\text{(g)} \quad \frac{\partial E_y}{\partial x} &= -\mu_0 \frac{\partial H_z}{\partial t} & \text{(h)} \quad \frac{\partial H_y}{\partial x} &= \frac{\partial D_z}{\partial t}
\end{aligned}$$

We can use the equations from (25) to conclude that  $D_x$  and  $H_x = 0$ . Therefore,  $D$  and  $H$  are perpendicular to the wave's direction of propagation. However, because we can no longer assume that  $E$  and  $D$  are parallel, the electric field can have a component which is perpendicular to the wave front.

The equations from (25) also tell us that, in a linearly polarized wave,  $E$ ,  $D$ , and the direction of the wave's propagation are coplanar. (Case 1)

And, if we make the assumption that  $\kappa_2$  and  $\kappa_3$  are equal, then  $E$ ,  $D$ , and the optics axis are coplanar (Case 2)

Given the above two cases, there are only two linearly polarized waves which satisfy both of the above cases.

- A wave with an electric vector perpendicular to the optic axis, called an “ordinary wave.”
- A wave with an electric vector that lies in the plane that contains the optics axis and the direction of propagation, called the “extraordinary wave.”

We can now consider the velocities of the extraordinary and ordinary waves, using the  $x$ -axis as the direction of propagation with the  $xz$ -plane containing the axis of the crystal. A  $v$ -axis (an arbitrary line perpendicular to the optic axis  $O_u$ ) is assumed to be coincident with the  $y$ -axis.

For an ordinary wave  $E_z = 0$ ,  $D_z = 0$ ,  $H_y = 0$ ,  $H_x = 0$ ,  $E_x = 0$ , and  $D_y = \kappa_2 \epsilon_0 E_y$ .

Therefore, equations (25 f, g) yield

$$(a) \quad \frac{\partial H_z}{\partial x} = -\kappa_2 \epsilon_0 \frac{\partial E_y}{\partial t} \quad (b) \quad \frac{\partial E_y}{\partial x} = -\mu_0 \frac{\partial H_z}{\partial t} \quad (26)$$

If we eliminate  $H_z$ , then

$$\frac{\partial^2 E_y}{\partial x^2} = \kappa_2 \epsilon_0 \mu_0 \frac{\partial^2 E_y}{\partial t^2} \quad (27)$$

Which we can identify as the equation for a wave traveling with the velocity

$$v = \frac{1}{\sqrt{\kappa_2 \epsilon_0 \mu_0}} = \frac{c}{\sqrt{\kappa_2}} \quad (28)$$

So the index of refraction for the ordinary wave is

$$n_2 = \sqrt{\kappa_2} \quad (29)$$

For the extraordinary wave  $E_y = 0$ ,  $D_y = 0$ ,  $H_z = 0$ ,  $H_x = 0$ ,  $D_x = 0$ , but  $E_x \neq 0$

Therefore we are left with only equations (25 e, h).

$$(a) \quad \frac{\partial E_z}{\partial x} = \mu_0 \frac{\partial H_y}{\partial t} \quad (b) \quad \frac{\partial H_y}{\partial x} = \frac{\partial D_z}{\partial t} \quad (30)$$

If we have  $\kappa$  equal to

$$\kappa = \frac{D_z}{\epsilon_0 E_z} \quad (31)$$

Then the above equations give

$$\frac{\partial^2 E_z}{\partial x^2} = \kappa \epsilon_0 \mu_0 \frac{\partial^2 E_z}{\partial t^2} \quad (32)$$

Which we can recognize as the equation of a wave traveling with velocity

$$v = \frac{1}{\sqrt{\kappa \epsilon_0 \mu_0}} = \frac{c}{\sqrt{\kappa}} \quad (33)$$

So the index of refraction of the extraordinary wave is

$$n = \sqrt{\kappa} \quad (34)$$

By taking the scalar product of  $\vec{E}$  and  $\vec{D}$ , recalling that both lie in the uw-plane, and using equation (31) we find,

$$\frac{1}{\kappa} = \varepsilon_0 \frac{E_z}{D_z} = \varepsilon_0 \frac{E_z D_z}{D_z^2} = \varepsilon_0 \frac{E_u D_u + E_w D_w}{|\vec{D}|^2} = \frac{1}{\kappa_1} \frac{D_u^2}{|\vec{D}|^2} + \frac{1}{\kappa_2} \frac{D_w^2}{|\vec{D}|^2} \quad (35)$$

If  $\chi$  is the angle between the u-axis (the optic axis) and the x-axis (the propagation direction), then equation (35) simplifies to

$$\frac{1}{\kappa} = \frac{\sin^2 \chi}{\kappa_1} + \frac{\cos^2 \chi}{\kappa_2} \quad (36)$$

The Poynting vector of the extraordinary wave

$$\vec{S} = \vec{E} \times \vec{H} \quad (37)$$

Represents the energy flux density, which is not perpendicular to the plane of the wave, because E is not in this plane. Instead, we can expect it to coincide with the direction of the ray, which lies in the plane containing the optic axis and the direction of propagation of the wave. The angle  $\beta$  between D and E and the same angle  $\beta$  between the direction of propagation and S lead to the relation

$$\tan \beta = \frac{(n_1^2 - n_2^2) \tan \chi}{n_1^2 + n_2^2 \tan^2 \chi} \quad (38)$$

This equation, along with the others leading up to it, show how H, D, E, S and the direction of propagation are all related to the indices of refraction  $n_1$  and  $n_2$  and the angle between the optical axis and the direction of propagation. In addition, they allow us to determine the way in which an electromagnetic wave will propagate through a

homogeneous, anisotropic dielectric. Practically, this is done by placing such a material between two crossed polarizers to determine if a well defined optical axis exists, and how it is distributed throughout the sample.

### *Superfluid $^3\text{He}$*

$^3\text{He}$ , in its pure form, has three superfluid phases:  $A_1$ , A, and B, all of which are BCS (Bardeen-Cooper-Schrieffer) condensates of p-wave ( $L = 1$ ) Cooper pairs [10] that form nuclear spin-triplet ( $S = 1$ ) states [11]. The superfluidity is a result of the formation of these Cooper pair of  $^3\text{He}$  particles. The  $A_1$  phase, which only exists in a magnetic field, is the magnetically-polarized state, and is the state that becomes superfluid at the highest temperature in a magnetic field. When there is no magnetic field, there are two stable phases: A and B. Many of the physical properties of the A (B) phase, for example, the susceptibility to magnetic fields, are anisotropic (isotropic). These features of pure  $^3\text{He}$  phases are well-defined, but these phases are altered in fundamental ways in the presence of an impurity such as aerogel.

When an impurity is introduced in superfluid  $^3\text{He}$  with high porosity silica aerogel, a metastable A-like phase has been shown to appear on cooling [12-15] This phase is thought to be like the A phase in bulk superfluid  $^3\text{He}$ , known to be the axial p-wave state., This metastable phase, at sufficiently low temperatures, will undergo a transition to an isotropic superfluid phase similar to the isotropic state observed in bulk  $^3\text{He}$ , the B phase. Upon warming, though, a distinct transition from the B-like phase to the A-like phase in aerogel is not seen. Tracking experiments [14-17] have shown that coexistence of A-like and B-like phases occurs in a narrow temperature window, approximately 20–50  $\mu\text{K}$ , near the normal-to-superfluid transition temperature in aerogel,  $T_{ca}$ . This is contrary to

the expectation that the B phase should be stable at all pressures and temperatures if the disorder introduced is homogenous and the scattering is isotropic<sup>1</sup>. However, scattering anisotropy from strands of aerogel may destabilize the B-like phase in favor of the A-like phase [18].

It has been suggested [17] that the introduction of global anisotropy into aerogel, for example, by uniaxial strain, might increase the stability of the A-like phase. Aoyama and Ikeda have recently calculated [19] that uniaxial anisotropy, which can be achieved by compression along one axis, should stabilize the axial state. Radial anisotropy, however, achieved by radial compression or by a radial reduction in the sample due to preferential shrinkage during growth, might stabilize the polar state. The ability to produce and characterize aerogels with these specific attributes, that is the motivation for this work.

## **Experiments and Discussion**

This experimental work is presented chronologically to show the development from one stage of research to the next.

### *Aerogel Growth*

Silica aerogels can be grown utilizing a variety of methods. At Northwestern, we have used a ‘two-step’ solvent exchange method and a ‘one-step’ sol-gel method outlined by Teichner [20]. Early difficulties largely were involved with aerogel shrinkage and cracking, as well as the inability to reproduce results.

In a ‘one-step’ sol-gel method, a silicon oxide precursor, tetramethyl orthosilicate (TMOS), is dissolved in methanol and hydrolyzed, and ammonia is used as a catalyst.

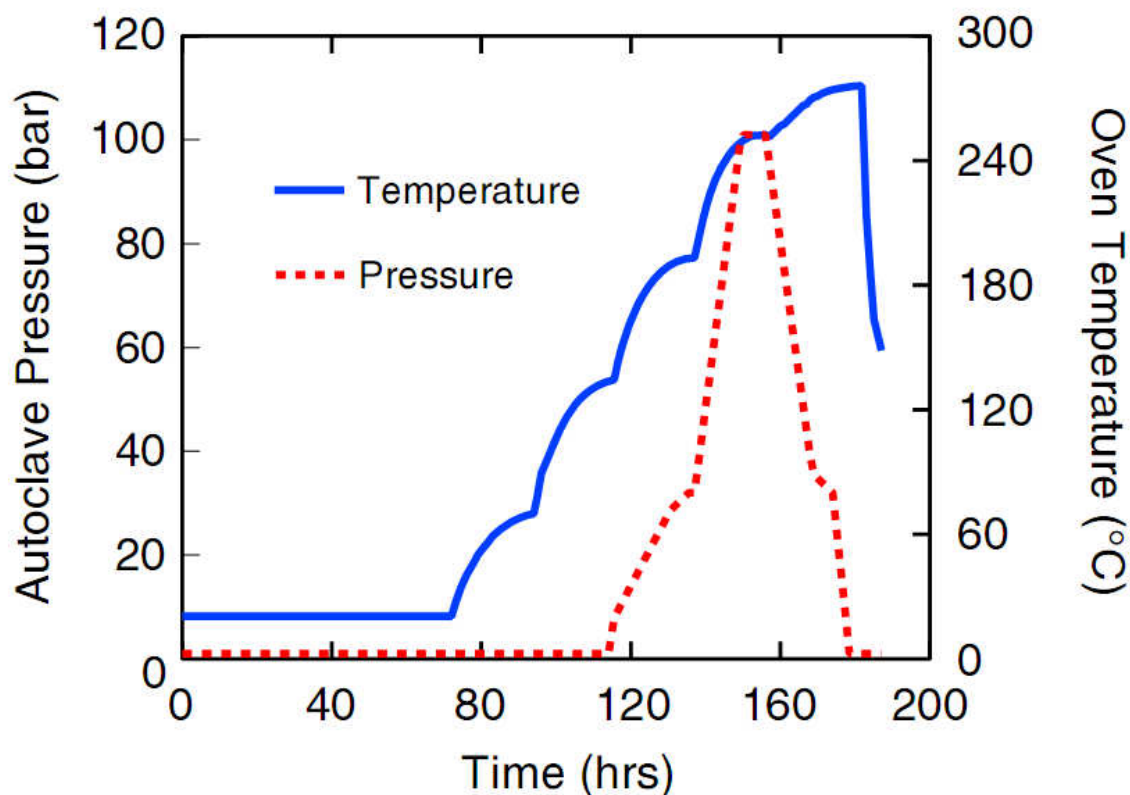


---

<sup>1</sup> E. V. Thuneberg, S. K. Yip, M. Fogelström, and J. A. Sauls, Phys. Rev. Lett. 80, 2861 (1998)

This reaction results in a wet gel, known as an alcogel. The alcogel is then supercritically dried following a method that is based on the rapid supercritical extraction process (RSCE) of Poco et al. [21]. Specifically, the sol, the combination of TMOS, methanol, water, and catalyst before gelation, is poured into a cylindrical stainless steel chamber that has an inner diameter of 5.08 cm and a length of 4.92 cm and contains glass tubes of various sizes as molds. The chamber can also be loaded with other devices made with, but not limited to, stainless steel, gold, quartz, and tantalum, but many materials, including brass, can alter the gel chemistry significantly, which leads to undesirable results. The chamber is completely filled with the sol and sealed using two stainless steel lids each having a thickness of 1.27 cm. Each lid is bolted in place using six 8-32 screws. The alcogel that forms is typically aged at room temperature for approximately three days. The chamber which contains the alcogel is then loaded into an autoclave which has an open volume of 0.46 L. 50 mL of methanol is then added into the open volume. The autoclave is loaded into an oven and heated through several manual adjustments and, as the temperature rises, the pressure in the alcogel chamber forces the lids to open slightly, allowing fluid to escape into the open volume of the autoclave. Once the critical point of methanol ( $T_c = 239.5\text{ }^\circ\text{C}$ ,  $p_c = 80.81\text{ bar}$ ) is exceeded the autoclave is emptied by slowly opening a high pressure valve. This drying typically begins from a starting temperature and pressure of  $\sim 270\text{ }^\circ\text{C}$  and  $\sim 100\text{ bar}$ . The system is depressurized  $\sim 8\text{--}12\text{ h}$  and then allowed to cool to room temperature overnight. Fig. 1 depicts the typical oven temperature and autoclave pressure profiles during aging and drying.

Fig. 1



The 'two-step' solvent exchange method uses TMOS, methanol, acetonitrile, and water, where hydrochloric acid (HCl) is used as a catalyst. In this method the acetonitrile must be solvent exchanged with methanol before the gel can be supercritically dried. We found that achieving reproducible results using this method was difficult, though it is very similar to the 'one-step' method. The solvent exchange adds additional days to the process, as the alcogel must form in the chamber before beginning the solvent exchange. This is because the solvent exchange process involves the removal of the stainless steel chamber lid in a methanol bath, which can damage the alcogel if it has not fully formed. Furthermore, the gel continues to age until it is dried, which means the reaction of the TMOS and water with the acetonitrile and acid catalyst can be compromised if the solvent exchange is done too early. The acid catalyst used in this process might also be

the source of problems with shrinkage and inhomogeneity in the gels. As shown in Fig. 2, the pH of the reaction controls hydrolysis and condensation rates, which are directly linked to the gel structure[22]. Acid catalysts can lead to a gel with a more polymeric structure, whereas a basic catalyst yields a colloidal one. Though the graph is for TEOS, tetraethyl orthosilicate, instead of for TMOS, the reaction principle remains the same.

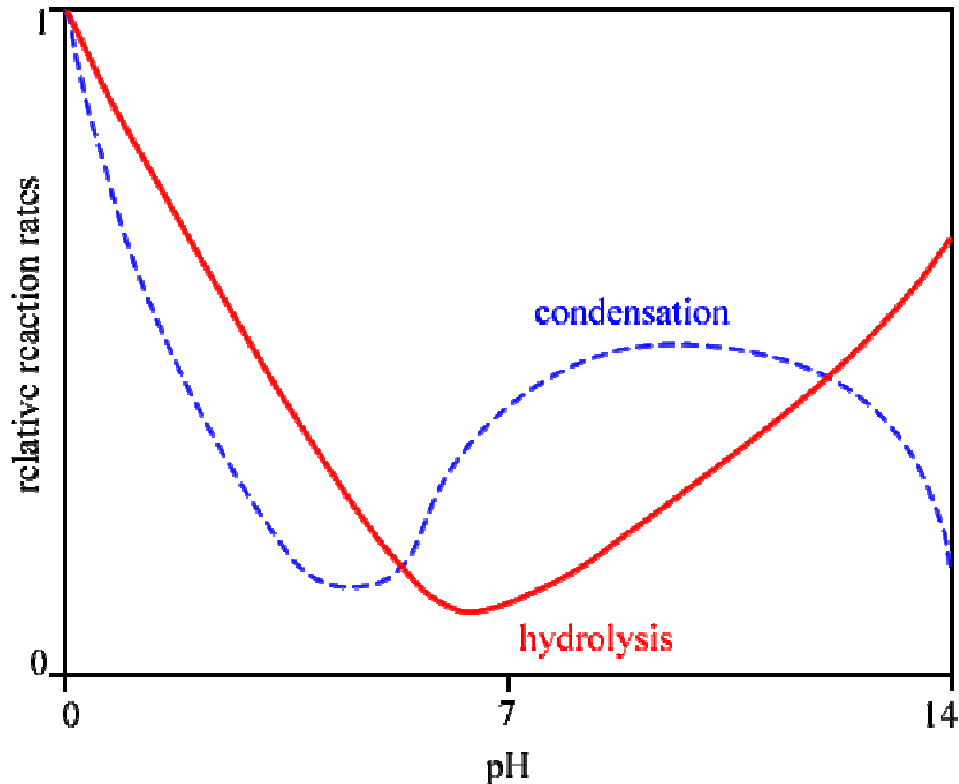


Fig. 2 - Hydrolysis and condensation of TEOS as a function of pH [Ref]

The decision to focus on 'one-step' aerogel growth was made given the difficulties associated with the 'two-step' method. To achieve consistency with 'one-step' growth, tests comparing the effect of different base catalyst concentrations were performed. A base concentration of 9 mL  $\text{NH}_4\text{OH}$  to 1 L  $\text{H}_2\text{O}$  was found to consistently produce a ~98%-98.5% porous gel with small amounts shrinkage using a ratio of:

**10 mL TMOS : 80 mL Methanol : 2.44 mL Ammonia-Water Solution**

With the one step method we have successfully produced silica aerogel ranging in porosity from ~94%–99%. A sample's porosity is determined from its weight and volume after supercritical drying to an accuracy of 0.1% for a 98% aerogel.

#### *Optical Birefringence Characterization of Aerogel*

To perform optical birefringence experiments on high porosity aerogels two linear polarizers, circular in geometry, each with indices indicating 5° of rotation up to 360° from the vertical polarization axis are used (see Fig. 3).

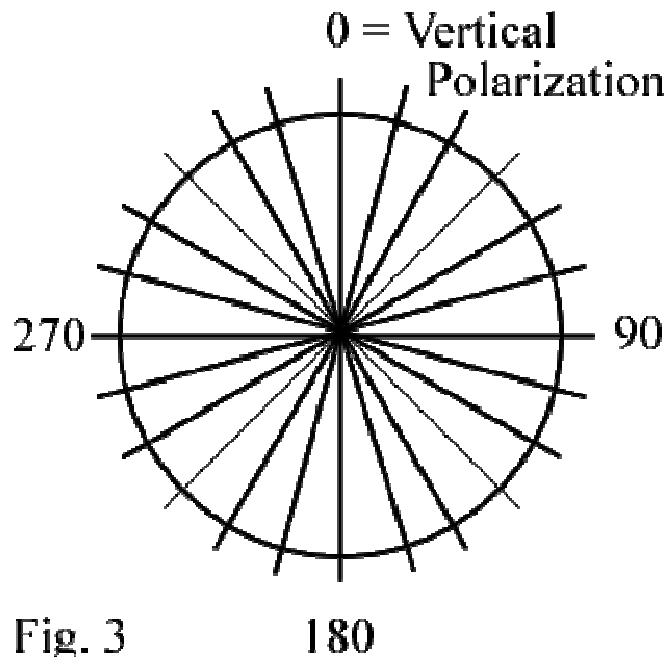


**Fig. 3** 180

These polarizers are placed on either side of a sample oriented 90° with respect to one another. White light is used to illuminate the polarizer-sample-polarizer array, but first passes through a diffusing filter, this is because the features of the light source itself (the filament emitting the light, for example) are distinguishable without the diffusing filter present. A camera is located after the polarizer furthest from the light source (Fig. 4).

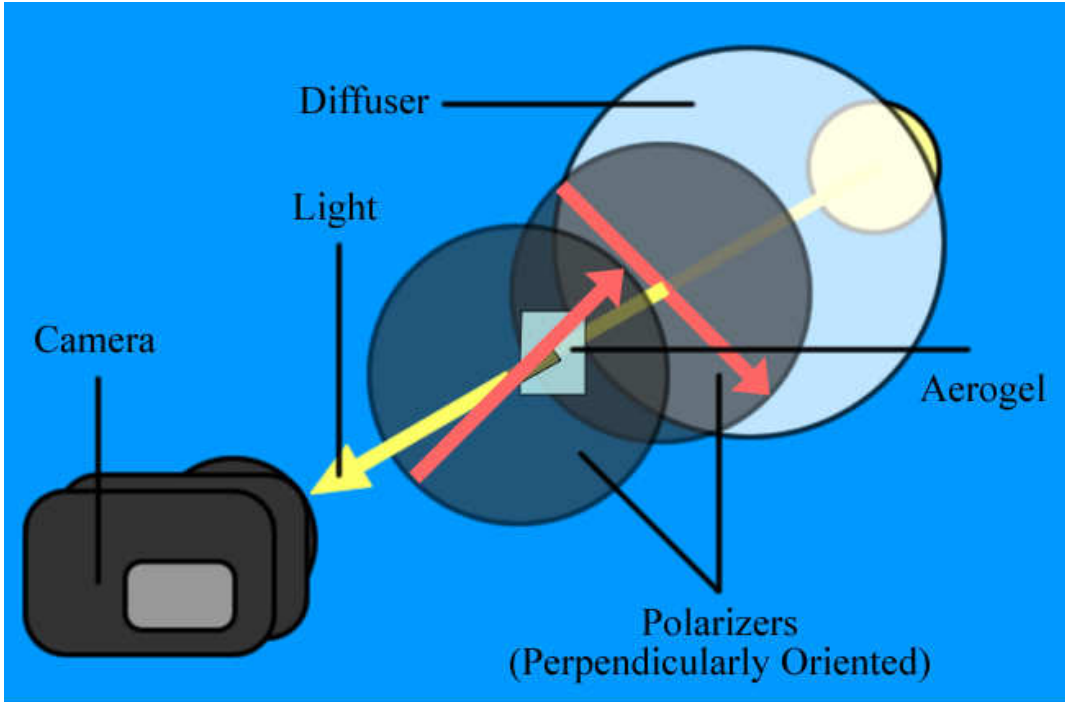


Fig. 4 - Cartoon of Optical Birefringence Setup

Intensity of light from pictures taken were plotted against the exposure time (given by the shutter speed) to ensure that camera was operating within a linear regime (Fig. 5).

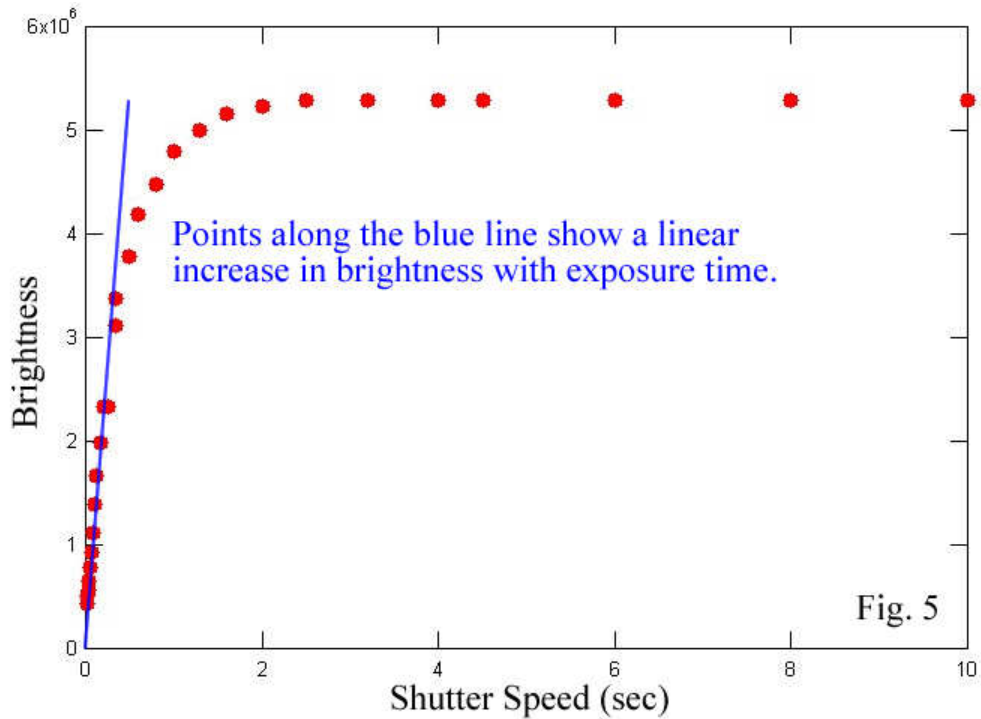


Fig. 5

Samples of aerogel characterized using this method showed both density variations, manifested as colors, and inhomogeneity, shown by dark and light regions appearing simultaneously when looked at through crossed polarizers. Isotropic regions appear dark for all orientations relative to the polarizers, while anisotropic regions will change continuously from light to dark and back, which indicates the optical axis (Fig. 6).



Fig. 6 - From left to right: an aerogel sample exhibiting both local density variations and anisotropy, an aerogel with inhomogeneously distributed anisotropy, an aerogel with an isotropic core and anisotropic surroundings

The discovery of such variety among the samples produced and preexisting samples can help to explain inconsistencies in superfluid  $^3\text{He}$  experiments done in the past. The ability to immediately characterize samples grown in the lab helped to motivate growth of aerogels with tunable anisotropy as well as homogeneity that would not only be useful in  $^3\text{He}$  experiments, but would directly correspond to theoretical predictions.

#### *Aerogel Samples for Superfluid $^3\text{He}$ Experiments*

As discussed previously, aerogel samples which exhibit homogeneous anisotropy both uniaxially or radially correspond to predictions of the stabilization of new phases in superfluid  $^3\text{He}$ . The instant feedback mechanism optical birefringence provided allowed for better understanding of the aerogel growth mechanisms. To produce a homogeneous, uniaxially anisotropic sample, a homogeneous, isotropic sample had to be created first. To produce this kind of sample, the ‘one-step’ growth method was used. The crucial

aspect to produce these samples was engineering appropriate boundary conditions within the chamber containing the alcogel. The flow of methanol out of this chamber during the drying process is a likely cause of anisotropy in the aerogel. Therefore, regions of the gel that experience isotropic fluid flow are more likely to be isotropic themselves.

Homogeneous, isotropic aerogels with ~98% porosity were grown utilizing these principles. (Pictures of these samples under optical birefringence are not shown, as the sample is black in every orientation.) Once homogeneous, isotropic aerogels were obtained, uniaxial compression of them was simple. Aerogels grown to be homogeneously radially anisotropic were grown in the same way, with the addition that catalyst concentration was systematically increased until the desired amount of shrinkage was obtained.

Fig. 7 shows optical birefringence of a 98% porosity aerogel as it was axially strained to 18.6% in 2.3% increments. The crossed polarizers were oriented with one polarizer at  $45^\circ$  and the other at  $135^\circ$  relative to the vertical cylinder axis of the gel. The sample did not exhibit any radial shrinkage after supercritical drying. Panel 1 of Fig. 7 indicates that the unstrained gel is homogeneously isotropic as described above. We have also found no transmission of light propagating down the cylinder axis for this isotropic aerogel when placed between crossed polarizers. Panels 2–9 of Fig. 7 demonstrate that strain can be used to effectively convert this nominally isotropic aerogel into a polarizer, which we attribute to optical birefringence. The polarization effect increases with increasing strain, the result of structural anisotropies on optical length scales. Furthermore, it is evident from the approximately uniform intensity of the image that this anisotropy is a global property of the entire sample and is homogeneously distributed.

From Fig. 7 we can measure the relative intensity of light passing through the sample averaged over a central region of the image of the aerogel as a function of strain. These results are presented in Fig. 8 and indicate that the transmitted intensity increases linearly with increasing strain up to the largest value of strain, 18.6%.

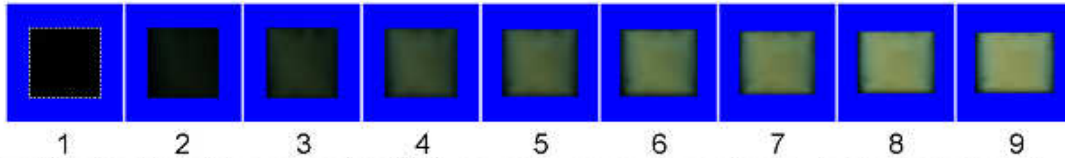


Fig. 7 Optical birefringence of a 98% porosity aerogel, nominally isotropic before it was subjected to increasing axial strain. The strain increases from left to right: 1 (unstrained), 2 (2.3% strain), 3 (4.7%), 4 (7.0%), 5 (9.3%), 6 (11.6%), 7 (14.0%), 8 (16.3%), 9 (18.6%)

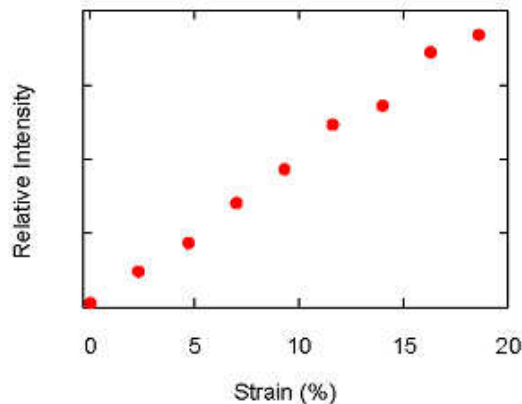


Fig. 8 Relative intensity averaged over a central region of the image of the sample versus strain for the sample presented in Fig. 7

By rotating both polarizers, keeping them crossed, we can determine the direction of the anisotropy axis. Fig. 9 presents such a rotation sequence for the sample at its maximum compression, i.e. 18.6%. The fact that the intensity maxima (minima) are seen when the polarizers are oriented at  $45^\circ$  and  $135^\circ$  ( $90^\circ$  and  $180^\circ$ ) is consistent with the anisotropy axis being oriented along the cylinder (strain), axis.

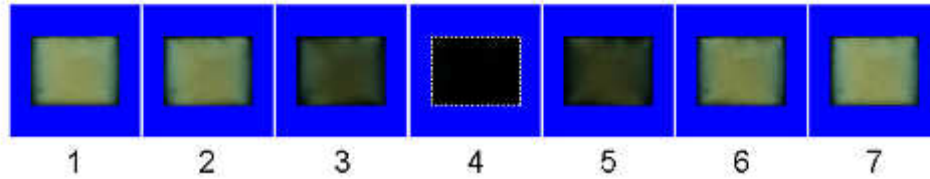


Fig. 9 Optical birefringence of a 98% porosity aerogel strained by 18.6%. The labels are associated with the rotation of the polarizers relative to the cylinder axis: 1 ( $45^\circ$ ,  $135^\circ$ ), 2 ( $60^\circ$ ,  $150^\circ$ ), 3 ( $75^\circ$ ,  $165^\circ$ ), 4 ( $90^\circ$ ,  $180^\circ$ ), 5 ( $105^\circ$ ,  $195^\circ$ ), 6 ( $120^\circ$ ,  $210^\circ$ ), 7 ( $135^\circ$ ,  $225^\circ$ )

Optical birefringence was also used to investigate possible intrinsic anisotropy in a sample exhibiting radial shrinkage. As before, the polarizers were initially oriented with one at  $45^\circ$  and the other at  $135^\circ$  relative to the cylinder axis. They were then rotated together, keeping them crossed. We have found that aerogels exhibiting radial shrinkage polarize transmitted light and this can be observed with cross polarizers, indicating the existence of a well defined optical axis. Again we attribute this effect to optical birefringence. Fig. 10 shows an aerogel cylinder which exhibits 12.7% radial shrinkage and shows that axial intrinsic anisotropy is present in the sample. It is noteworthy that this intrinsic anisotropy seems to be less uniform throughout the sample than that induced by strain as displayed in panels 2, 3, 5, and 6 of Fig. 10. For the intrinsically anisotropic samples, i.e. those exhibiting radial shrinkage, we observed only a small amount of transmission through crossed polarizers for light propagating down the cylinder axis. This, along with the rotation series presented in Fig. 10, indicates that the cylinder axis is predominantly the optical axis in the case of samples exhibiting anisotropy due to radial shrinkage.

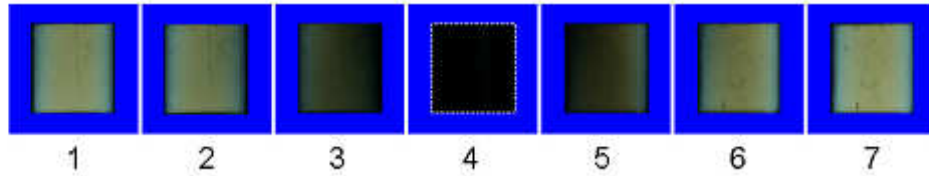


Fig. 10 Optical birefringence of a 98% porosity aerogel exhibiting 12.7% radial shrinkage. The labels are associated with the rotation of the polarizers relative to the cylinder axis: 1 ( $45^\circ$ ,  $135^\circ$ ), 2 ( $60^\circ$ ,  $150^\circ$ ), 3 ( $75^\circ$ ,  $165^\circ$ ), 4 ( $90^\circ$ ,  $180^\circ$ ), 5 ( $105^\circ$ ,  $195^\circ$ ), 6 ( $120^\circ$ ,  $210^\circ$ ), 7 ( $135^\circ$ ,  $225^\circ$ )

## Conclusion

The aerogel growth and characterization methods discussed here provide a useful and necessary tool for performing experiments on superfluid  $^3\text{He}$ . Additionally, the ability to grow aerogels of specific characteristics has implications for applications in a wide array of physical systems. Bhupathi et al., for example, have suggested that uniaxially strained aerogels can be used to make waveplates [23]. Optical birefringence gives a clear picture of the principal directions of the anisotropy on optical length scales and has the advantage of displaying an image that shows the homogeneity of this anisotropy as it is distributed over the sample. The technique has been complemented by data from x-ray scattering, further discussion of which can be found in Pollanen et al. [24]. Furthermore, some aerogel samples grown using these techniques have already been implemented in experiments. For example, Davis et al. used transverse acoustic impedance methods to study  $^3\text{He}$  in an aerogel compressed 17% uniaxially [25]. To conclude, the aerogel growth and characterization methods presented have allowed, and will continue to allow, for new and relevant experiments on superfluid  $^3\text{He}$  to be performed.

## **Acknowledgements**

I would like to thank Prof. Bill Halperin, without whom I would not have been able to embark on this fascinating, often frustrating, but very rewarding research over the past few years. I have sincerely enjoyed my time in the ultra low temperature lab, and it has inspired me to continue to do graduate work in condensed matter physics. Second, I would like to thank Andy Rivers who, from the day I arrived at Northwestern, has provided me with great guidance and advice. I would especially like to thank Johannes Pollanen, who has been a great coworker and friend. Thanks to Bill Gannon, Charles Collett, Andrew Fang, Ben Rolfs, Hyungsoon Choi, John Davis, Leo Li, and Satoshi Sasaki, who have all added their own charm to the lab. Last, and most importantly, I would like to thank my girlfriend Kari, my parents, brother, and the rest of my family, who support me in whatever I do, and who are proud of me even when I ram a broken pipette into my thumb.

## References

- [1] J. Fricke, *Sci. Am.* **258** (5) (1988) 92
- [2] M. Reim, W. Korner, J. Manara, S. Korder, M. Arduini-Schuster, H.-P. Ebert, and J. Fricke, *Solar Energy* **79** (2) (2005) 131.
- [3] J.B. Miller, S.E. Rankin, E.I. Ko, *J. Catal.* **148** (1994) 673
- [4] D.W. Schaefer, K.D. Keefer, *Phys. Rev. Lett.* **56** (1986) 2199
- [5] L.W. Hrubesh, T.M. Tillotson, J.F. Poco, in: B.J.J. Zelinski, C.J. Brinker, D.E. Clark, D.R. Ulrich (Eds.), *Better Ceramics Through Chemistry IV*, MRS Symposia Proceedings No. 180, Materials Research Society, Pittsburgh, 1990, p. 315.
- [6] J. Baker, *Science* **314** (5806) (2006) 1707
- [7] M. Cantin, M. Casse, L. Koch, R. Jouan, P. Mestreau, D. Roussel, C. Saclay, F. Bonnin, J. Moutel, S.J. Teichner, *Nucl. Instrum. Methods* **118** (1974) 177
- [8] G.W. Gray, *Molecular Structure and the Properties of Liquid Crystals* (Academic, New York, 1962)
- [9] D.A. Balzarini, *Phys. Rev. Lett.* **25** (1970) 914
- [10] W.P. Halperin, G. Gervais, K. Yawata, N. Mulders, *Physica B* **329**, 288 (2003)
- [11] D. Vollhardt and P. Wölfle, *The Superfluid Phases of Helium 3*, (Taylor and Francis, London, 1990)
- [12] B. I. Barker, Y. Lee, L. Polukhina, D. D. Osheroff, L. W. Hrubesh, and J. F. Poco, *Phys. Rev. Lett.* **85**, 2148 (2000)
- [13] G. Gervais, T. M. Haard, R. Nomura, N. Mulders, and W. P. Halperin, *Phys. Rev. Lett.* **87**, 035701 (2001)
- [14] G. Gervais, K. Yawata, N. Mulders, and W. P. Halperin, *Phys. Rev. B* **66**, 054528 (2002)
- [15] E. Nazaretski, N. Mulders, and J. M. Parpia, *JETP Lett.* **79**, 383 (2004)
- [16] J. E. Baumgardner, Y. Lee, D. D. Osheroff, L. W. Hrubesh, and J. F. Poco, *Phys. Rev. Lett.* **93**, 055301 (2004)
- [17] C. L. Vicente, H. C. Choi, J. S. Xia, W. P. Halperin, N. Mulders, and Y. Lee, *Phys. Rev. B* **72**, 094519 (2005)
- [18] E. V. Thuneberg, S. K. Yip, M. Fogelström, and J. A. Sauls, *Phys. Rev. Lett.* **80**, 2861 (1998)
- [19] K. Aoyama and R. Ikeda, *Phys. Rev. B* **73**, 060504 (R) (2006)
- [20] S.J. Teichner, in: J. Fricke (Ed.), *Aerogels: Proceedings of the First International Symposium, Würzburg, Fed. Rep. of Germany, September 23–25, 1985*, (Springer, Berlin, New York, 1985), p. 22
- [21] J.F. Poco, P.R. Coronado, R.W. Pekala, L.W. Hrubesh, in: R.F. Lobo, J.S. Beck, S.L. Suib, D.R. Corbin, M.E. Davis, L.E. Iton, S.I. Zones (Eds.), *Microporous and Mesoporous Materials, MRS Symposium Proceedings, vol. 431*, (Materials Research Society, Pittsburgh, PA, 1996), p. 297.
- [22] H. Schmidt and H. Scholze, in: J. Fricke (Ed.), *Aerogels: Proceedings of the First International Symposium, Würzburg, Fed. Rep. of Germany, September 23–25, 1985*, (Springer, Berlin, New York, 1985), p. 49.
- [23] P. Bhupathi, J. Hwang, R. M. Martin, J. Blankstein, L. Jaworski, N. Mulders, D. B. Tanner, and Y. Lee: submitted to *Optics Express* (2009); arXiv:0905.1118v1
- [24] J. Pollanen, K. R. Shirer, S. Blinstein, H. Choi, T. M. Lippman, W. P. Halperin, and L.B. Lurio, *J. Non-Crystalline Solids* **354** 4668 (2008)

- [25] J.P. Davis, J. Pollanen, B. Reddy, K.R. Shirer, H. Choi and W.P. Halperin, Phys. Rev. B. **77** 140502(R) (2008)
- [26] H. Römer, *Theoretical Optics: An Introduction*. (Wiley-VCH, Darmstadt, 2005)
- [27] B. Rossi, *Optics*. (Addison-Wesley Publishing Company, Inc., Massachusetts, 1957)
- [28] M. Born and E. Wolf, *Principles of Optics: Electromagnetic Theory of Propagation Interference and Diffraction of Light*. (Cambridge University Press, Cambridge , 1997)
- [29] J. Fricke and T. Tillotson, *Thin Solid Films* **297** (1997) 212
- [30] W.P. Halperin and J.A. Sauls, arXiv:cond-mat/0408593v1, (2004)
- [31] W.P. Halperin, H. Choi, J.P. Davis and J. Pollanen, J. Phys. Soc. Jpn. **77** 11, 111002 (2008)